



CHORUS

This is the accepted manuscript made available via CHORUS. The article has been published as:

Reentrance of low-temperature nonmetallic phase of $\text{La}_{\{2/3\}}\text{Sr}_{\{1/3\}}\text{MnO}_{\{3\}}$ (110) thin films

Lin Li, Zhaoliang Liao, Zhenyu Diao, Rongying Jin, E. W. Plummer, Jiandong Guo, and
Jiandi Zhang

Phys. Rev. Materials **1**, 034405 — Published 22 August 2017

DOI: [10.1103/PhysRevMaterials.1.034405](https://doi.org/10.1103/PhysRevMaterials.1.034405)

Reentrance of Low-Temperature Nonmetallic Phase of $\text{La}_{2/3}\text{Sr}_{1/3}\text{MnO}_3$ (110) Thin Films

Lin Li^{1,2}, Zhaoliang Liao², Zhenyu Diao², Rongying Jin², E. W. Plummer², Jiandong Guo¹, and Jiandi Zhang^{2*}

¹*Institute of Physics, Chinese Academy of Sciences, Beijing 100190*

²*Department of Physics and Astronomy, Louisiana State University, Baton Rouge, LA 70810, USA*

Abstract

We have studied $\text{La}_{2/3}\text{Sr}_{1/3}\text{MnO}_3$ thin films grown on (3×1) -reconstructed SrTiO_3 (110) substrates. Films with thicknesses less than the critical thickness of $\theta_c \cong 8$ unit cells are insulating in the measured temperature (T) range (2 - 400 K). However, films with thicknesses slightly over θ_c exhibit reentrant nonmetallic behavior at low temperatures in addition to the normally observed metal-insulator transition at higher temperatures. In contrast, the magnetization doesn't show signs of low- T transitions. Such reentrance of a low- T nonmetallic phase is affected by the film thickness as well as the density of oxygen vacancies. The electrical resistivity analysis reveals that localization effects are responsible for the reentrant nonmetallic behavior, which is enhanced with reduced film thickness.

PACS number(s): 71.30.+h, 71.27.+a, 73.20.Fz, 73.50.-h

*jiandiz@lsu.edu

Manganites have attracted tremendous attention due to their exotic properties such as “colossal magnetoresistance” [1], high spin polarization [2] and charge/orbital ordering phenomena [3]. Such exotic behaviors in this class of materials are thought to arise from the intimate coupling between lattice, spin, charge and orbital degrees of freedom, which results in a series of competing ground and low-lying excited states. Delicate balance between these competing states can be further tuned by the introduction of reduced dimensionality [4,5], strain [6,7] and broken symmetry at interfaces [8,9], enabling the artificial designs of novel functionalities.

Doped $\text{La}_x\text{Sr}_{1-x}\text{MnO}_3$ ($x = 1/3$, $\text{La}_{1/3}\text{Sr}_{2/3}\text{MnO}_3$, referred to as LSMO thereafter), an itinerant ferromagnetic metal with almost 100% spin-polarization at Fermi energy [2] and a Curie temperature (T_C) of about 370 K [10], is a promising material for future device applications [11-13]. However, LSMO in thin film form becomes insulating when the films are thinner than a critical thickness, which is usually called the dead layer [14]. This is fatal for the performance of LSMO based devices. Extensive efforts have been put into understanding the origin of the dead layer and several mechanisms have been proposed, such as orbital reconstruction at the interface [15-16], strain imposed by the substrate [17], phase separation [18-19], and interface polar discontinuity [20]. Element intermixing across the interface might play an important role since the doping level of $\text{La}_x\text{Sr}_{1-x}\text{MnO}_3$ significantly affects its T_C and conductivity [21]. Additionally, impurities and defects should be considered [22], as they may induce localization effects which are strong in low dimensional materials [5, 23]. All these factors are normally coupled with each other and likely enhanced at the hetero-interfaces of artificial oxide structures, making the problem even more complicated [9].

Many LSMO film studies are mainly focused on films epitaxially grown along the (001) direction. Epitaxial LSMO films with the (110) and (111) directions add another complex issue related to the interface polarity while the underlying physics can be related to interface geometric and electronic structures [24]. The surfaces of the substrates such as (110) and (111) SrTiO_3 (STO) are polar, which will strongly affect

the growth and interface properties of films. Here we report our investigation of transport properties of LSMO ultrathin films grown on STO (110) substrates where no polar discontinuity occurs across LSMO/STO interface [24]. In addition to the metal-insulator transition (MIT) that directly defines the dead layer, we observe reentrant behavior of a nonmetallic state at temperatures lower than the T_C of the LSMO films with the thickness slightly higher than the critical thickness of the dead layer. The electrical resistivity measurements of the reentrant nonmetallic phase show the characteristics of strong localization, which becomes important in materials with reduced dimensionality (thickness).

Figure 1(a) schematically shows lattice structure of ultrathin LSMO films epitaxially grown on STO (110). The LSMO films were grown on single crystalline STO (110) substrates. For *in-situ* surface STM and LEED characterization, 0.5 wt% Nb-STO (110) substrates were used while non-doped substrates, which are insulating and thus more suitable for transport measurements of the grown films, were chosen for *ex-situ* electrical resistivity and magnetic properties characterization. The substrates were first annealed in vacuum at 900 °C for 1 hour and then annealed at 700 °C in a 10 mTorr ozone atmosphere for 30 min. Ozone gas used here is O₂ mixed with 2 wt% O₃. As shown in Fig. 1(b), the *in-situ* STM image of the Nb-STO surface shows that the surface has atomically flat terraces. A (3×1) reconstruction is formed on the surface according to both the patterns of reflective high-energy electron diffractions (RHEED) in Fig. 1(c) and low energy electron diffraction (LEED) in Fig. 1(d). The bright and sharp spots in the LEED image further indicate that the surface is well ordered. The surface with the (3×1) reconstruction has been well studied [25]. It is terminated by fully-coordinated TiO₆ units and is expected to be chemically inert. We also found that the (3×1) reconstruction is stable at 700 °C in both vacuum and an oxygen atmosphere (partial pressure from 10⁻⁶ Torr to 130 mTorr). On such a substrate the LSMO films were grown by pulsed laser deposition (PLD) in ozone with a laser fluence of $\sim 1 \text{ J cm}^{-2}$ and a substrate temperature of 700 °C. High quality, layer-by-layer growth was achieved with different oxygen partial pressures (P_{O})

ranging from 10^{-6} Torr to 130 mTorr. Previous report also demonstrated a coherent growth of LSMO films on STO (110) substrates [24]. Figure 1e shows an example of the RHEED intensity oscillation for a 8 unit cells (u.c.) film grown at 80 mTorr where one oscillation is corresponding to one u.c. growth. For (110) orientation, one u.c. is 2.74 Å. The thicknesses of the films are precisely controlled by counting the RHEED intensity oscillation. The corresponding STM image of the surface of a LSMO film with 8 u.c. indicates that it is atomically flat (see Fig. 1f). In contrast to the (3×1) reconstructed substrate, the film shows a (1×1) RHEED and LEED pattern [see Fig. 1(g) and 1(h)]. The real time RHEED pattern monitor shows that the (3×1) RHEED pattern changed to (1×1) just after the growth of 1 u.c. LSMO began.

The T -dependence of the electrical resistivity of LSMO films grown with $P_O = 80$ mTorr is shown in Fig. 2(a). The 60-u.c.-thick film shows metallic behavior with a T_P

$$\left[\left(\frac{d\rho}{dT} \right) \Big|_{T=T_p} = 0 \text{ and } \left(\frac{d^2\rho}{dT^2} \right) \Big|_{T=T_p} < 0 \right]$$

is quantitatively consistent with the bulk value [21]. On the other hand, the films become less conductive and T_P decreases with reducing film thickness. Eventually the films become insulating in the measured temperature range as the thickness is reduced to 8 u.c. or thinner. We thus define a critical thickness ($\theta_c \cong 8$ u.c.) for the dead layer of LSMO on STO (110). This value of θ_c is different from that for LSMO grown under similar optimal growth conditions on STO (001) (with $\theta_c = 6$ u.c.) in terms of u.c. [26], but their real thickness is almost identical [2.2 nm for (110) and 2.3 nm for (001) films]. In contrast to the LSMO/STO (001) interface, there is no polar discontinuity across the (110) LSMO/STO interface [24]. Thus, no charge transfer is expected. Further, it is reported that the charge transfer is also very limited for the $\text{La}_{1-x}\text{Sr}_x\text{MnO}_3/\text{STO}$ interface with optimized doping of $x = 1/3$ [27]. In contrast, both scanning transmission electron microscopy (STEM) and X-ray diffraction have shown a tilt relaxation of MnO_6 octahedra starting from the interface in (001) oriented LSMO films grown on NdGaO_3 and SrTiO_3 substrates due to interfacial octahedral coupling which retains the connectivity of octahedra across the interface of two

different perovskite materials [28-31]. The relaxation of the octahedra results in a thickness dependent lattice constant [29,30,32] and transport properties [29,32]. Regarding to the LSMO films grown on STO (110) substrates, H. Boschker et al. has also reported a higher out-of-plane lattice constant c with reduced film thickness [33]. Since interfacial octahedral coupling occurs as well at the (110) LSMO/STO interface, the observed reduced T_P with decreasing thickness in our (110) LSMO films may also be related to the change of lattice structure.

Interestingly, films slightly thicker than the dead layer (e.g., 9 or 10 u.c. thick) exhibit an upturn in resistivity at low temperatures, reentering into nonmetallic behavior. Here we refer it as a metal to nonmetal crossover at temperature T_V

($\left. \frac{d\rho}{dT} \right|_{T=T_V} = 0$ and $\left. \frac{d^2\rho}{dT^2} \right|_{T=T_V} > 0$) [see Fig. 2(a)], in contrast to T_P as defined for the

insulator-metal transition at high temperatures which usually is accompanied by ferromagnetic (FM) to paramagnetic (PM) phase transitions at T_C that are normally observed in LSMO [21]. For the 9 u.c. film, T_V is ~ 65 K and its resistivity increases by ~ 10 times at 2 K as compared to that at 65 K. Such a drastic upturn of the resistivity at low temperatures is not observed in thicker films such as the films of 11 u.c. or thicker. It can be concluded that the reentrance of the nonmetallic state at low temperatures is thickness dependent, mainly occurring in the films with thickness close to the critical thickness.

Furthermore, the observed thickness dependence of the reentrant nonmetallic behavior can almost be reproduced by varying the oxygen deficiency in a film with a thickness close to the formation of the dead layer. It has been reported that oxygen vacancies (V_O) suppress the metallicity of LSMO (001) films and increase the dead layer thickness [26]. We have adjusted the V_O density in the LSMO (110) films by changing the ozone partial pressure during growth, and also found that the films become more nonmetallic with decreasing P_O (i.e., increasing V_O density). Compared to the film grown with $P_O = 80$ mTorr, the $P_O = 1 \times 10^{-6}$ Torr film has a dead layer of 12 u.c.. The reentrant T_V is also related to P_O . As shown in Fig. 2b, the 9-u.c.-thick film grown at

60 mTorr shows an MIT with $T_P = 140$ K, and reenters into the nonmetallic phase at $T_V = 67$ K. Other films grown at higher P_O (80 mTorr and 130 mTorr) show higher T_P but lower T_V . By annealing the sample at 750 °C in 250 mTorr ozone gas for 1 hour, T_V can be further lowered to 48 K. At low P_O (1×10^{-6} Torr, 8 mTorr, and 40 mTorr), the 9-u.c.-thick films are insulating through the measured temperature range, and exhibit no reentrance behavior. In brief, a lower V_O concentration drives the film to be more metallic and suppresses the reentrance behavior.

To understand the origin of the low- T nonmetallic phase, we have compared the T -dependence of their magnetic and electrical properties. As indicated by the T -dependent magnetization and magnetization hysteresis loop (see Fig. 3), the 9-u.c.thick film grown at 80 mTorr is ferromagnetic at low temperatures with $T_C = 181$ K, coincident with its MIT critical temperature T_P . This is understood within the picture of a double-exchange (DE) interaction that mediates the coupling between metallicity and ferromagnetism [34]. On the other hand, unlike the sharp upturn of the resistivity corresponding to the reentrant nonmetallic phase at T_V , the magnetization increases monotonically with decreasing temperature below T_C . All the LSMO (110) films exhibit qualitatively the same magnetization characteristics, indicating that the reentrant nonmetallic phase does not have a magnetic origin.

A summary of the effects of thickness and oxygen vacancy concentration on the electrical transition temperature and magnetic transition is shown in Fig. 4. The T_P and T_C will decrease with decreasing thickness, while T_V increases with decreasing thickness. A slight difference between T_P and T_C is observed which could be due to the fact that other effects such as polaron [35-37] and phase separation [38,39] rather than double exchange [34] alone also affect the electron transport. When the T_P or T_C crosses over with T_V , the metallic phase completely disappears. Since the T_C still survives in 7 and 8 u.c. films, a ferromagnetic phase coexists with the nonmetallic phase, which is inconsistent with a DE interaction mechanism [34]. Changing the oxygen partial pressure P_O has similar effects on the trend of T_P and T_V . The T_P is reduced while T_V is enhanced with decreasing P_O and finally tend to converge, after

which the dead layer develops. Such changes between the T_P and T_V indicate two competing effects which relate to disorder-induced localization and DE interaction, which will be discussed later.

Reentrance into a nonmetallic phase for the 8-u.c.-thick LSMO film grown on (001)-oriented $(\text{LaAlO}_3)_{0.3}(\text{SrAl}_{0.5}\text{Ta}_{0.5}\text{O}_3)_{0.7}$ (LSAT) has been observed, which seems to be related to the phase separation occurring at low- T [40]. However, in the current work on LSMO (110) films, the observed continuous increase of magnetization below T_C clearly indicates a monotonic increase of the ferromagnetic domains upon cooling. Therefore, the possibility of phase separation being the dominant origin of the reentrance behavior can be ruled out. The picture of thermal activated transport is not supported either since the resistivity below T_V of the 9-u.c.-thick LSMO film does not fit into the Arrhenius plot $\ln(\rho) \propto T^{-1}$. Instead, the upturn of the resistivity at T_V must be considered as induced by localization effects of carriers.

As shown in Fig. 5(a), the T -dependence of resistivity for the 9-u.c.-thick LSMO film grown with $P_O = 80$ mTorr exhibits the characteristic of Mott's variable range hopping (VRH), fit with $\rho = \rho_0 \exp(T_0 / T)^\alpha$ (ρ_0 and T_0 are constants, respectively) below T_V with exponent $\alpha = 1/3$, as expected for two dimensional materials [22, 41]. A nonzero density of states at the Fermi level would be expected [41]. At temperatures between T_P and T_V , the carriers may be activated into extended states driving the film metallic, while above T_P (T_C) the metallic transport is suppressed since the ferromagnetic order is broken.

The thickness dependence of T_V is also of primary importance. For films grown under the same conditions (as-grown with $P_O = 80$ mTorr) in which the densities of V_O (as well as chemical disorders) were kept unchanged, T_V decreases upon increasing thickness from 9 to 15 u.c. (see Fig. 4). Transport analysis below T_V reveals that $\rho(T)$ of the 9/10-u.c.-thick films follows the VRH model, while the 11/15-u.c. films show weak localization [42] behavior [i.e., $\rho(T) \propto \log(T)$], as illustrated in Fig. 5(a) and 5(b). The localization is enhanced with reducing film thickness as reflected by the

change in the slope of $\rho(T)$ versus $\log(T)$, resulting in the enhanced stability of the nonmetallic phase and, accordingly, the increased T_V .

Due to the dominant role of disorder-induced localization, a large negative magnetoresistance (MR) is observed at low temperatures below T_V . As shown in Fig. 6, negative MR is observed for a 9 u.c. LSMO film under 7 T and 14 T fields. The MR ratio $|\rho(H) - \rho(0)|/\rho(0)$ shows a peak around T_P , which is normally observed for manganite films in the presence of a strong magnetic field which forces spins to be aligned in parallel and thus increases the electron hopping rate due to the DE interaction [21]. However, note that the MR is enhanced below T_V where the film is already in its FM phase. Since negative MR due to spin-alignment with the field will normally decrease with decreasing temperature, the observed enhanced negative MR below T_V has to originate from the field-induced destruction of localization [43]. Therefore, the enhanced negative MR further confirms that disorder-induced localization is the origin for the low- T reentrant nonmetallic phase.

With advanced PLD techniques, the thickness of LSMO films can be varied with the precision of a single unit cell and the desired film stoichiometry can be achieved by optimizing the growth parameters. This is of special interest for the control of V_O because the dependence of the saturation of the metal-insulator transition temperature for the (001) LSMO films upon the oxygen gas partial pressure during growth [26] shows the minimization of V_O concentration. In contrast to (001) orientation, the polar (110) orientation would favor the formation of oxygen vacancies near surface to avoid polar catastrophe [44]. Our LSMO films possess a (1x1) surface structure, suggesting that the surface polarity is compensated by the formation of oxygen vacancies near the surface. Furthermore, chemical disorder is always present for a randomly doped LSMO. Those disorders will induce localization effects that are further enhanced in films with reduced film thickness.

Consequently, T_V increases with decreasing thickness. Since both the T_C and T_P decrease with decreasing thickness [14, 26], T_P and T_V will crossover each other when

the film is at or below the critical thickness. Even though the ferromagnetic order that promotes the metallic phase is formed in the film, the strong localization effects may keep it nonmetallic.

In summary, the LSMO films grown on SrTiO₃ (110)-(3×1) show a thickness-induced MIT with a critical thickness ($\theta_c \cong 8$ u.c) normally referred to as a dead layer. At a lowered temperature, films slightly thicker than the dead layer reenter the nonmetallic phase. Localization is observed in the electrical transport, and is enhanced with reducing film thickness. By varying oxygen partial pressure we reveal the systematic evolution of the two transition temperatures with V_O density, including the crossover from weak to strong localization. Besides V_O , the unavoidable chemical disorder of the doped LSMO is also a source of localization, resulting in the intrinsic limitation of reducing the dead layer thickness.

Acknowledgements:

The research was primary supported by US DOE under Grant No. DOE DE-SC0002136. L.L. and J.D.G. acknowledge financial support from Chinese Natural Science Foundation (Nos. 11474334 & 11634016). J.Z. acknowledge the sabbatical program of the institute of physics. Chinese Academy of Science.

References

1. Y. Tokura, *Rep. Prog. Phys.* **69**, 797 (2006).
2. J.-H. Park, E. Vescovo, H.-J. Kim, C. Kwon, R. Ramesh, T. Venkatesan, *Nature* **392**, 794 (1998).
3. Elbio Dagotto, *Science* **309**, 257 (2005).
4. A.V. Boris, Y. Matiks, E. Benckiser, A. Frano, P. Popovich, V. Hinkov, P. Wochner, M. Castro-Colin, E. Detemple, V. K. Malik, C. Bernhard, T. Prokscha, A. Suter, Z. Salman, E. Morenzoni, G. Cristiani, H.-U. Habermeier, B. Keimer, *Science* **332**, 937 (2011).
5. R. Scherwitzl, S. Gariglio, M. Gabay, P. Zubko, M. Gibert, and J.-M. Triscone, *Phys. Rev. Lett.* **106**, 246403 (2011).
6. D. Pesquera, G. Herranz, A. Barla, E. Pellegrin, F. Bondino, E. Magnano, F. Sánchez, J. Fontcuberta, *Nat. Commun.* **3**, 1189 (2012).
7. T. Z. Ward, J. D. Budai, Z. Gai, J. Z. Tischler, Lifeng Yin & J. Shen, *Nat. Phys.* **5**, 885 (2009).
8. E. W. Plummer, Ismail, R. Matzdorf, A.V. Melechko, J. P. Pierce, Jiandi Zhang, *Surf. Sci.* **500**, 1–27 (2002).
9. H. Y. Hwang, Y. Iwasa, M. Kawasaki, B. Keimer, N. Nagaosa, and Y. Tokura, *Nature Mater.* **11**, 103 (2012).
10. Y. Tokura and Y. Tomioka, *J. Magn. Magn. Matter.* **200**, 1 (1999).
11. J. O'Donnel, A. E. Andrus, S. Oh, E.V. Colla, D.N. Eckstein, *Appl. Phys. Lett.* **76** (1914) 2000.
12. A. Fert, A. Barthélémy, J. Ben Youssef, J.-P. Contour, V. Cros, J.M. De Teresa, A. Hamzic, J.M. George, G. Faini, J. Grollier, H. Jaffrès, H. Le Gall, F. Montaigne, F. Pailloux, F. Petroff, *Mater. Sci. Eng. B* **84**, 1 (2001).
13. T. Yajima, Y. Hikita, & H. Y. Hwang, *Nat. Mater.* **10**, 198 (2011).
14. M. Huijben, L. W. Martin, Y. -H. Chu, M. B. Holcomb, P. Yu, G. Rijnders, D. H. A. Blank, and R. Ramesh, *Phys. Rev. B* **78**, 094413 (2008).

15. A. Tebano, C. Aruta, S. Sanna, P. G. Medaglia, G. Balestrino, A. A. Sidorenko, R. De Renzi, G. Ghiringhelli, L. Braicovich, V. Bisogni, and N. B. Brookes, *Phys. Rev. Lett.* **100**, 137401(2008).
16. A. Tebano, A. Orsini, P. G. Medaglia, D. Di Castro, G. Balestrino, B. Freelon, A. Bostwick, Young Jun Chang, G. Gaines, E. Rotenberg, and N. L. Saini, *Phys. Rev. B.* **82**, 214407 (2011).
17. M. Angeloni, G. Balestrino, N. G. Boggio, P. G. Medaglia, P. Orgiani and A. Tebano, *J. Appl. Phys.* **96**, 6387(2004).
18. M. Bibes, L. Balcells, S. Valencia, J. Fontcuberta, M. Wojcik, E. Jedryka, and S. Nadolski, *Phys. Rev. Lett.* **87**, 67210 (2001).
19. T. Becker, C. Streng, Y. Luo, V. Moshnyaga, B. Damaschke, N. Shannon, and K. Samwer, *Phys. Rev. Lett.* **89**, 237203 (2002).
20. H. Boschker, J. Verbeeck, R. Egoavil, S. Bals, G. van Tendeloo, M. Huijben, E. P. Houwman, G. Koster, D. H. A. Blank, and G. Rijnders, *Adv. Funct. Mater.* **22**, 2235–2240 (2012).
21. A. Urushibara, Y. Moritomo, T. Arima, A. Asamitsu, G. Kido, and Y. Tokura, *Phys. Rev. B* **51**, 14103 (1995).
22. B. Kramer and A. Mackinnon, *Rep. Prog. Phys.* **56**, 1496-1564 (1993).
23. S. Datta, *Electronic Transport in Mesoscopic Systems* (Cambridge University Press, 1997).
24. Er-Jia Guo, Timothy Charlton, Haile Ambaye, Ryan D. Desautels, Ho Nyung Lee, and Michael R. Fitzsimmons, *ACS Appl. Mater. Interfaces* **9**, 19307 (2017).
25. J.A. Enterkin, A.K. Subramanian, B.C. Russell, M.R. Castell, K.R. Poeppelmeier and L.D. Marks, *Nat. Mater.* **9**, 245 (2010)
26. Z. Liao, F. Li, P. Gao, L. Li, J. Guo, X. Pan, R. Jin, E. W. Plummer, and Jiandi Zhang, *Phys. Rev. B* **92**, 125123 (2015).
27. Julia A. Mundy, Yasuyuki Hikita, , Takeaki Hidaka,, Takeaki Yajima, Takuya Higuchi, Harold Y. Hwang, David A. Muller, & Lena F. Kourkoutis, *Nature Communications* **5**, 3464 (2014).
28. Z.L. Liao, M. Huijben, Z. Zhong, N. Gauquelin, S. Macke, R. Green, S. van Aert,

- J. Verbeeck, G. Van Tendeloo, K. Held, G. A. Sawatzky, G. Koster & G. Rijnders, *Nature Materials* **45**, 425 (2016).
29. Z.L. Liao, N. Gauquelin, R.J. Green, S. Macke, J. Gonnissen, S. Thomas, Z. Zhong, L. Li, L. Si, S. van Aert, P. Hansmann, K. Held, J. Xia, J. Verbeeck, G. Van Tendeloo, G.A. Sawatzky, G. Koster, M. Huijben, G. Rijnders, *Adv. Funct. Mater.* **27**, 1606717 (2017).
30. A. Vailionis, H. Boschker, Z.L. Liao, J.R.A. Smit, G. Rijnders, M. Huijben, G. Koster, *Appl. Phys. Lett.* **105**, 131906 (2014).
31. E. J. Moon, P. V. Balachandran, B. J. Kirby, D. J. Keavney, R. J. Sichel-Tissot, C. M. Schlepütz, E. Karapetrova, X. M. Cheng, J. M. Rondinelli, and S. J. May, *Nano Letters* **14**, 2509 (2014).
32. J. Z. Sun, D. W. Abraham, R. A. Rao and C. B. Eom, *Appl. Phys. Lett.* **74**, 3017 (1999);
33. H. Boschker, J. Kautz, E. P. Houwman, W. Siemons, D. H. A. Blank, M. Huijben, G. Koster, A. Vailionis, and G. Rijnders, *Phys. Rev. Lett.* **109**, 157207 (2012).
34. Zener, *Phys. Rev.* **82**, 403 (1951).
35. A. J. Millis, P. B. Littlewood, and B. I. Shraiman, *Phys. Rev. Lett.* **4**, 5144 (1995).
36. J.-S. Zhou, J. B. Goodenough, A. Asamitsu, Y. Tokura, *Phys. Rev. Lett.* **79**, 3234 (1997).
37. C. P. Adams, J. W. Lynn, Y. M. Mukovskii, A. A. Arsenov, and D. A. Shulyatev, *Phys. Rev. Lett.* **85**, 3954 (2000).
38. E. Dagotto, A. Moreo, and T. Hotta, *Physics Reports* **344**, 1 (2001).
39. M. Uehara, S. Mori, C. H. Chen, and S. W. Cheong, *Nature* **399**, 560, (1999).
40. B. Kim, D. Kwon, T. Yajima, C. Bell, Y. Hikita, B.G. Kim, and H.Y. Hwang, *Appl. Phys. Lett.* **99**, 092513 (2011).
41. W. Brenig, G. H. Dohler, and H. Heyszenau, *Philos. Mag.* **27**, 1093 (1973).
42. P. A. Lee and T. V. Ramakrishnan, *Rev. Mod. Phys.* **57**, 287 (1987).
43. G. Bergmann, *Phys. Rep.* **107**, 1 (1984).
44. F.M Li, F. Yang, Y. Liang, S.M. Li, Z.Z. Yang, Q.H. Zhang, W.T. Li, X.T. Zhu, L.

Gu, J.D. Zhang, E. W. Plummer, and J.D. Guo, *AIP Advances* 7, 065001 (2017).

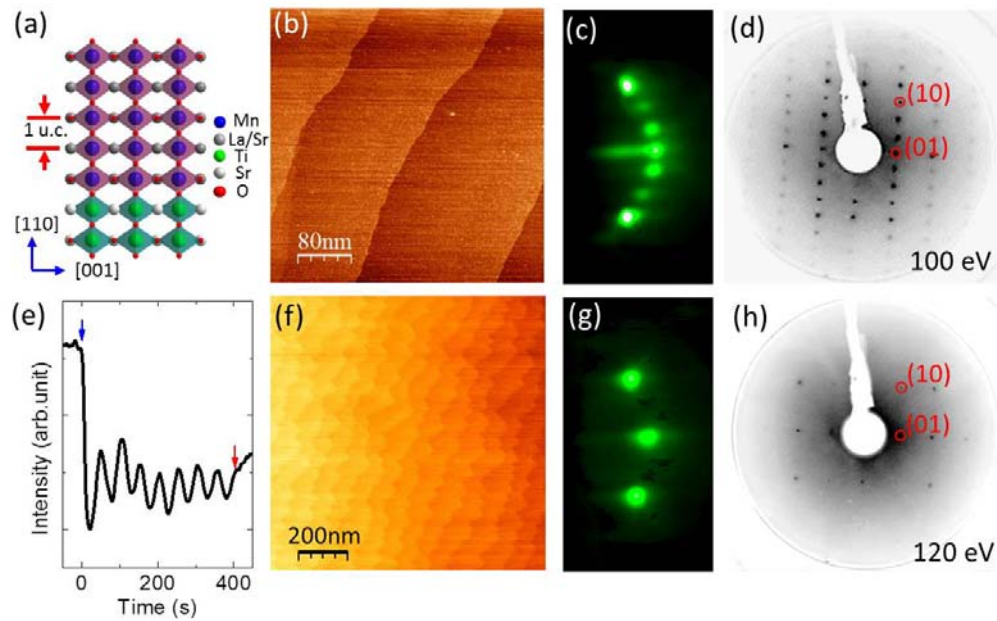


Figure 1 (a) Schematic structure model of LSMO on STO (110) substrate. STM image, RHEED, and LEED patterns of (b)-(d) the STO (110) substrate and (f)-(h) an 8 u.c. LSMO film grown at oxygen pressure $P_0 = 80$ mTorr, respectively. The beam energy for acquiring the LEED image and integer diffraction spots are indicated in panel (d) and (h). (e) RHEED intensity oscillation during the growth of 8 u.c. LSMO on STO (110) substrate at 80 mTorr. The blue and red arrows indicate the start and end of the growth, respectively.

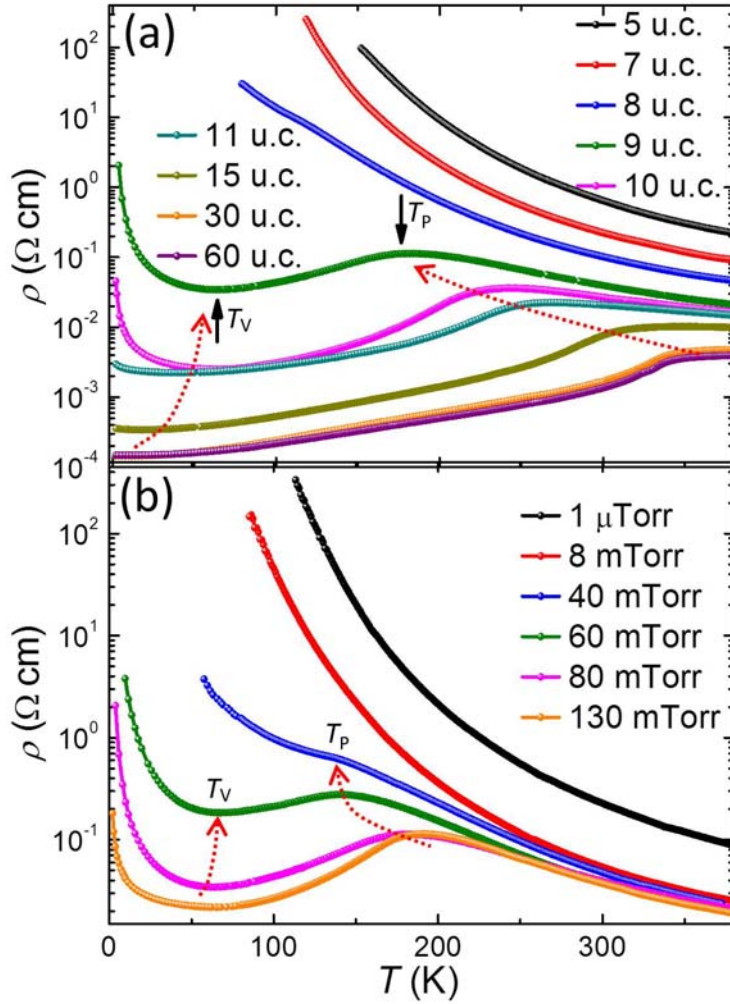


Figure 2 T -dependent resistivity of LSMO films **(a)** grown at 80 mTorr with different thickness and **(b)** with 9 u.c. thickness grown at different oxygen pressure. In (a) the black arrows illustrate the definition of the T_V (valley temperature, the critical temperature for metal-nonmetal crossover at low temperature) and T_P (peak temperature, the critical temperature for non-metal to metal crossover at high temperature). The dashed red arrows indicate the trend of the change of T_V and T_P with changing thickness (a) and pressure (b).

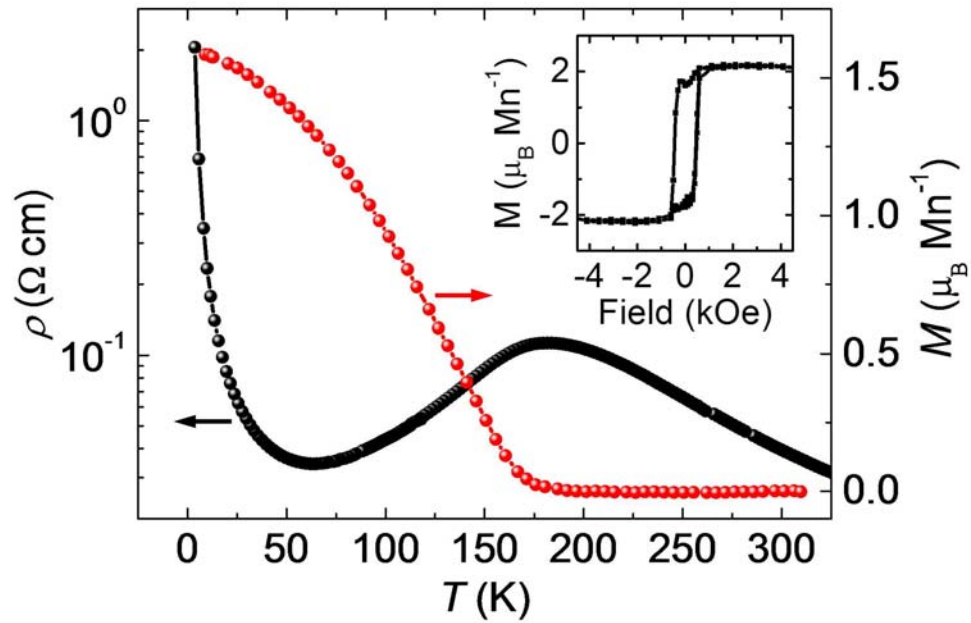


Figure 3 T -dependent resistivity and magnetization of the 9 u.c. LSMO film grown at $P_{\text{O}} = 80$ mTorr. The inset shows the ferromagnetic hysteresis loop at 10 K. The magnetization (M) was measured at 150-Oe after 1-T field cooling from 350 K.

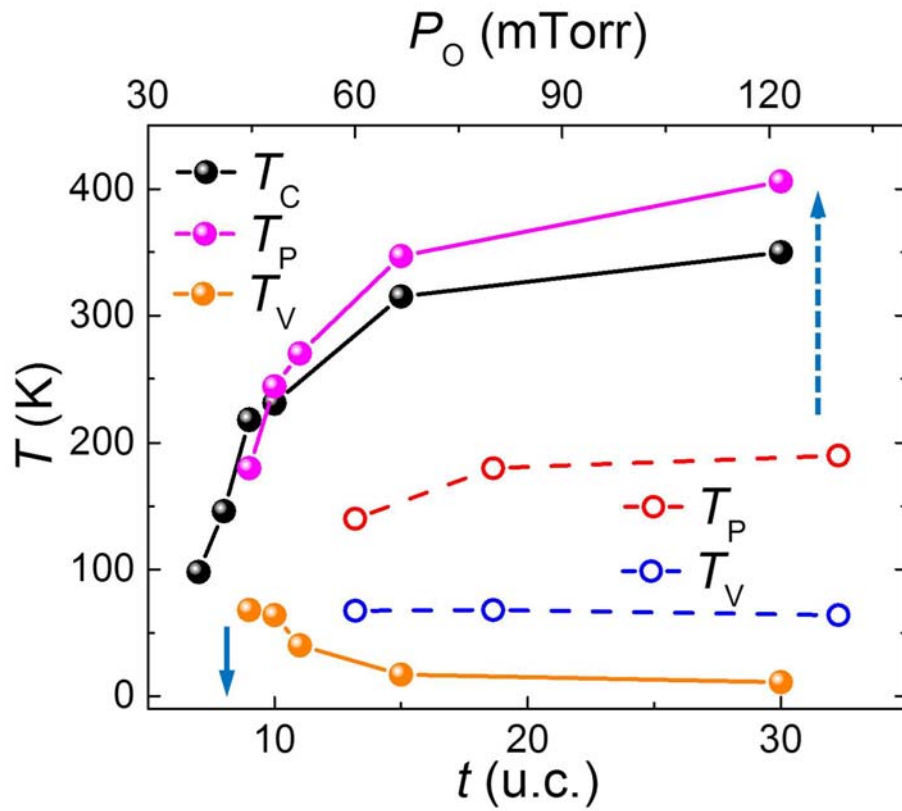


Figure 4 Thickness (t)- and P_O -dependent critical temperatures (T_p , T_v and T_c) of LSMO films. Solid symbols are for films with different thickness and open symbols for films grown at different oxygen partial pressures.

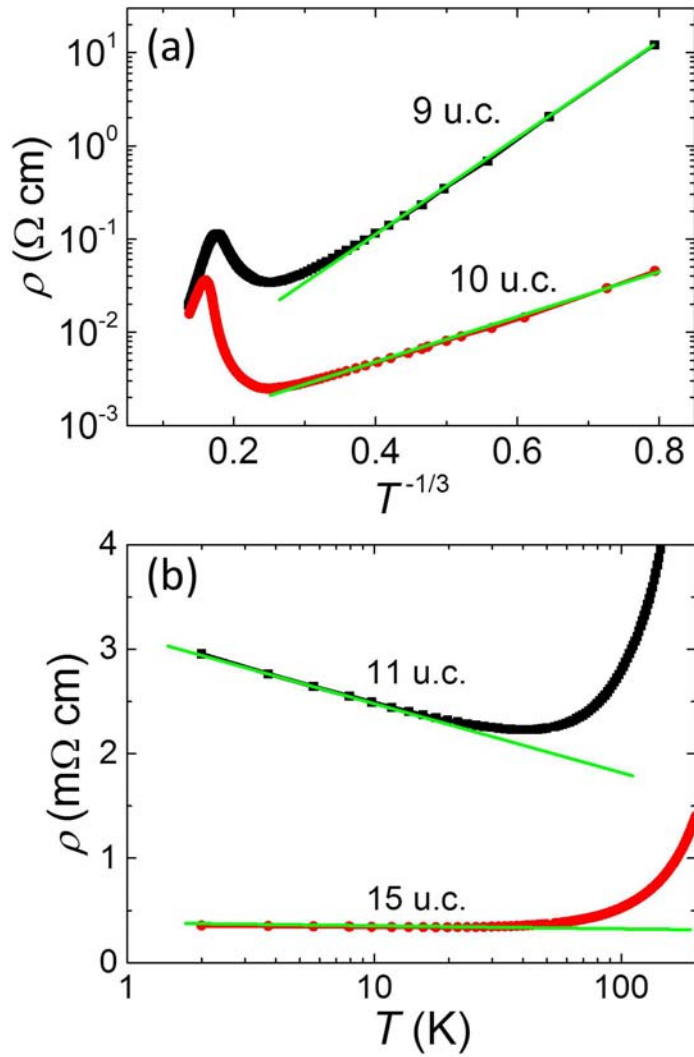


Figure 5 Low- T resistivity of the films grown at $P_O = 80$ mTorr with different thickness. (a) Log plot of resistivity as a function of $1/T^{1/3}$ for 9 u.c. and 10 u.c. films; (b) the resistivity versus $\text{Log}(T)$ for 11 u.c. and 15 u.c. films.

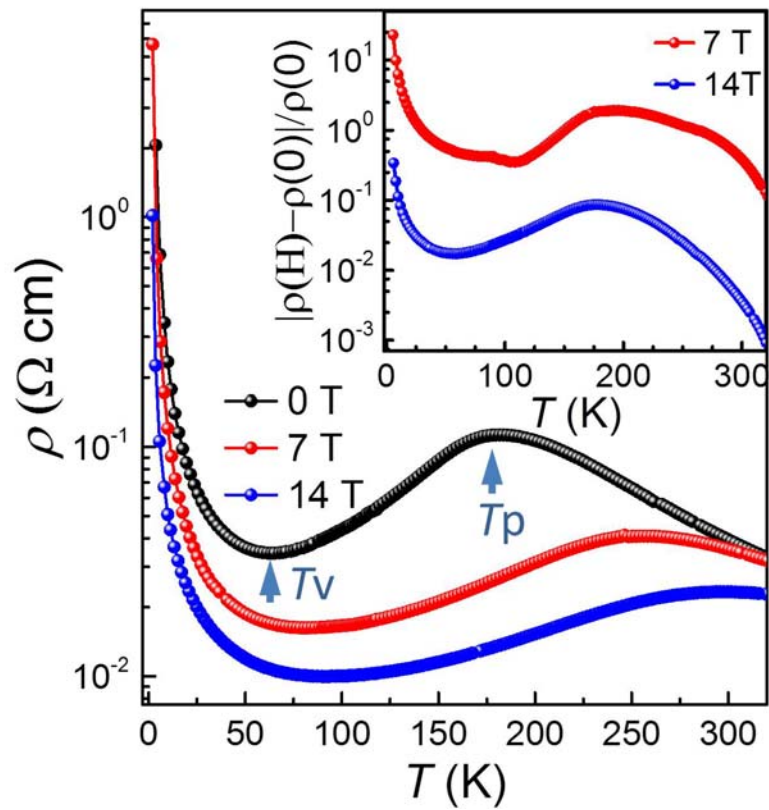


Figure 6 T -dependence of resistivity of a 9 u.c. LSMO film on STO (110) grown at $P_{\text{O}} = 80$ mTorr under different magnetic field. Inset shows the data of magnetoresistance $|\rho(H) - \rho(0)| / \rho(0)$.